

1 AERYN: a simple standalone application for visualizing and enhancing elemental maps

2

3 Vincent Mouchi\*<sup>1,2</sup>, Quentin G. Crowley<sup>1</sup> and Teresa Ubide<sup>1,3</sup>

4

5 <sup>1</sup>: Department of Geology, School of Natural Sciences, Trinity College Dublin, Museum Building,

6 College Green, Dublin 2, Republic of Ireland

7 <sup>2</sup>: Current address: Sorbonne Universités, UPMC Univ. Paris 06, CNRS UMR 7193, ISTeP, F-75005,

8 Paris, France

9 <sup>3</sup>: Current address: The University of Queensland, Brisbane QLD 4072, Australia

10

11 \*: corresponding author: vmouchi@gmail.com

12

13 Abstract

14 Interpretation of high spatial resolution elemental mineral maps can be hindered by high frequency

15 fluctuations, as well as by strong naturally-occurring or analytically-induced variations. We have

16 developed a new standalone program named AERYN (Aspect Enhancement by Removing Yielded

17 Noise) to produce more reliable element distribution maps from previously reduced geochemical data.

18 The program is Matlab-based, designed with a graphic user interface and is capable of rapidly

19 generating elemental maps from data acquired by a range of analytical techniques. A visual interface

20 aids selection of appropriate outlier rejection and drift-correction parameters, thereby facilitating

21 recognition of subtle elemental fluctuations which may otherwise be obscured. Examples of use are

22 provided for quantitative trace element maps acquired using both laser ablation (LA-) ICP-MS and

23 electron probe microanalysis (EPMA) of the cold-water coral *Lophelia pertusa*. We demonstrate how

24 AERYN allows recognition of high frequency elemental fluctuations, including those which occur

25 perpendicular to the maximum concentration gradient. Such data treatment compliments commonly

26 used processing methods to provide greater flexibility and control in producing elemental maps from

27 micro-analytical techniques.

28

29 Keywords: LA-ICP-MS; EDS; WDS; element distribution maps; processing; Matlab; biominerals.

30

## 31 1. Introduction

32 Element distribution maps or images acquired using in-situ analytical techniques are widely used in  
33 Geology and Earth Sciences (e.g. Cusack et al., 2008; Rittner & Müller, 2012; McGowan et al., 2014).

34 Several software packages exist to process element distribution maps (Paul et al., 2012; Rittner &  
35 Müller, 2012; Ortolano et al., 2014), with some recent studies having investigated multi-trace element  
36 maps processed from data obtained by laser ablation inductively coupled plasma mass spectrometry  
37 (LA-ICP-MS) (e.g. Petrus & Kamber, 2013; Paul et al., 2014; Ubide et al., 2015).

38 Common issues in micro-analytical techniques linked to data acquisition, such as analytical drift and  
39 outliers, can greatly influence the quality of resultant elemental maps. We propose a user-friendly  
40 method created using the programming software Matlab (MathWorks;  
41 <http://www.mathworks.com/products/matlab>) to deconvolute complex data and produce more  
42 readable elemental maps. LA-ICP-MS data must have been previously reduced to account for baseline  
43 correction and reference material calibration, e.g. by using common data reduction software. Our  
44 program, which we term AERYN (Aspect Enhancement by Removing Yielded Noise), allows the  
45 filtering of outliers and smoothing of values included in a data matrix, resulting in an increased  
46 readability and importantly permitting more representative and accurate interpretation of  
47 heterogeneity in elemental distribution. In addition, we propose a de-trending option to highlight  
48 subtle geochemical features which may be obscured by strong signal fluctuations, either natural in  
49 origin or caused by instrumental drift. AERYN has been compiled and exported as a standalone  
50 application for Windows, allowing its use on a PC without the requirement of a Matlab licence  
51 (<http://www.tcd.ie/Geology/staff/crowleyq/AERYN/>). The only requirement for this program to  
52 perform correctly is to download and install the free Matlab Runtime R2015a (8.5) from the  
53 MathWorks website (<http://www.mathworks.com/products/compiler/mcr>).

54 To illustrate how AERYN operates, we present elemental maps acquired by LA-ICP-MS and electron  
55 probe microanalysis (EPMA) from the wall of the skeleton of the cold-water coral *Lophelia pertusa*.

56 Virtually any type of numeric compositional map can use part or all of the protocol described here, as

57 long as the data fit to a square or rectangular shape (in laser-based systems, this can be achieved by  
58 analysing either parallel equivalent line scans or a grid of regularly-spaced spots). We provide the  
59 corresponding Matlab code and the standalone application as well as a "Read Me" file with some  
60 specifications as supplementary material, allowing the software to be adapted by other users.

61

## 62 2. AERYN description

### 63 2.1 User interface

64 AERYN is presented with a control panel on the left-hand side and three graphic areas on the right-  
65 hand side (Fig. 1). The upper graphic displays an elemental map (using Matlab's "imagesc" function)  
66 whereas the lower-left graphic displays a 3-dimensional view of the data (using Matlab's "surf"  
67 function). The lower-right graph represents a histogram of the data (number of bins calculated using  
68 Yule's rule) to graphically illustrate the distribution of elemental concentration represented in the  
69 other graphic displays.

70

### 71 2.2 Importing data

72 AERYN uses text files (.txt, .tsv) exported from a variety of elemental map processing software or  
73 from Microsoft Excel. We tested exports from LA-ICP-MS, Scanning Electron Microscopy with  
74 electron-dispersive spectroscopy (SEM-EDS) and EPMA maps, but text files from any software  
75 should be compatible. If not, we advise the user to follow instructions provided in the "Read Me" file.

76 AERYN does not process raw data, and a preceding data reduction step is still required. We used  
77 Iolite (Paton et al., 2011; v. 2.5 and 3.0) for data reduction prior to importing in AERYN. To import  
78 the numeric matrix corresponding to the map file, AERYN passes any number of lines composed of  
79 characters and reads only the part of the file containing the concentration values. The size of the  
80 imported matrix is only restricted by computer performance for very large datasets.

81 Once a numeric matrix has been generated, it is automatically displayed as a map on the upper graph  
82 and as a 3D surface plot of the 2D data on the lower-left graph (Fig. 1). It is therefore possible to  
83 rotate the lower-left graph or to automatically orient the view to a side section, in order to have better  
84 visibility of outliers and fluctuations. Moreover, if required for better display, it is possible to

85 transpose the matrix by clicking on "Transpose" in order to invert lines with columns.  
86 From this point and at any stage, the user can cancel any number of operations made on the data by  
87 clicking on the "Undo" button.

88

### 89 2.3 Outlier removal

90 Outliers can be either extremely high or low values in comparison to the rest of the observed data and  
91 introduce bias in interpretations. AERYN allows the user to locate and remove all outliers at once. All  
92 removed outliers are replaced by empty spaces in the matrix (NaN). Processing of these spaces is  
93 explained in the following section. A statistical test is proposed to the user to define automatic  
94 thresholds of outliers based on the following equations (Tukey, 1977; Carling, 2000):

95 (1)  $T_{up} = P90 + 1.5 * IQR$

96 (2)  $T_{down} = P10 - 1.5 * IQR$

97 With P90 the percentile at 0.90 for the dataset, P10 the percentile at 0.10 and  $IQR = P90 - P10$ . All  
98 values not occurring within the interval between  $T_{down}$  and  $T_{up}$  are considered as dataset outliers.  
99 Such a statistical treatment will likely be sufficient for most datasets, though for the data presented  
100 here the cut is too drastic and the upper end of some high value areas is lost, preventing an accurate  
101 reading of the corresponding concentrations. For this reason, a second technique, based on iterative  
102 visual definition of outliers, is made available for the user.

103 Firstly, for the high value outliers, it is necessary to estimate the upper limit of data to be retained. For  
104 this, the "surf" function of Matlab is extremely powerful. By displaying the elemental map in 3D on  
105 the lower-left graph (with the concentrations in the z axis) and with the possibility of rotating the  
106 image, one can clearly (i) identify variations in concentration, (ii) assess the potential presence of  
107 trends that would require a correction at a later stage, and (iii) identify obvious outliers and their  
108 approximate values. At this stage, successive outlier removal steps can be achieved by searching for  
109 values in the dataset lower or higher than a chosen specific value (Fig. 2). Moreover, the histogram on  
110 the third graph (lower-right area) allows a better estimate of the minimum and maximum values to be  
111 chosen for the colour palette in order to highlight most of the compositional information.

112 Spatially-restricted high concentration areas are maintained as a whole with this method, though more

113 subjectively compared to the automatic definition of outliers as presented above. It should be noted  
114 that a possibility of inadvertently “over-trimming” the dataset exists, especially when controlled by  
115 the user, and therefore outlier removal should be done with caution (e.g., Fig. 2c).

116 For the second phase of outlier removal, a lower minimum limit value expected for quantitative or  
117 semi-quantitative data is zero. This minimum value can be higher if the concentrations of the studied  
118 elements are high, but in the present example the concentrations are low and can easily be cut to  
119 positive values without further consideration. If the mapped area is not entirely filled with sample  
120 material (i.e., if a sample was mounted in epoxy resin and this resin was intentionally ablated in order  
121 to obtain a rectangular map), the user must ensure that the resin value, which is generally constant, is  
122 still included in the data to prevent incorrect resampling of these areas by the outlier removal step.

123 This step can have multiple iterations as successive outlier removals allow an improved visualisation  
124 of geochemical fluctuations. The automatic Side View is extremely valuable at this stage as the outlier  
125 values as well as the signal to be retained are indicated by the vertical axis. During the whole process  
126 however it is necessary to keep in mind that some valuable geochemical information can reside in  
127 high-frequency variability. It is thus unwise to crop the highest or lowest values too close to the main  
128 visible fluctuations (see Fig. 2a and caption). Moreover, one must be aware that the larger the holes  
129 caused by outlier removal, the less accurate the following steps will become. We suggest that the  
130 number of outliers compared to the size of the data must be reasonably low. As an indication, the  
131 number of points removed in Figure 2 represent approximately 0.5 % of the dataset (see Fig. 2c).

132 Each time the user filters the dataset, a temporary message is displayed in the history box to indicate  
133 the percentage of data cropped compared from the entire matrix. The cut values are displayed on the  
134 map as white areas. Once outlier removal has been validated, the side view and the histogram can  
135 provide preliminary boundaries for the colour palette (Fig. 2b). The filters can be cancelled to retain  
136 the entire initial dataset while maintaining the palette range values.

137

#### 138 2.4 Filling gaps following outlier removal

139 In the outlier removal step, the outliers have been automatically replaced by the specific passive value  
140 NaN. The "inpaint\_nans" function (D'Errico, 2004) allows replacement of NaNs by analyzing

141 surrounding values for interpolation and extrapolation. With this step completed, the maps are  
142 efficiently “cleaned” of outliers.  
143 This gap-filling step should not be performed after further steps such as smoothing, as the method  
144 used here substantially increases the number of NaN values in direct connection to pre-existing NaN  
145 values. For this reason, we chose to automatically fill the NaNs at the validation of the outlier  
146 removal.

147

## 148 2.5 Smoothing

149 An option to perform median filtering is available at this stage of data correction. Numerous  
150 smoothing functions and methods are available in the Matlab environment. In order to take into  
151 account the possible variability present on both x and y axes, the "medfilt2" function was chosen. This  
152 function calculates the mean of all values included in a moving square centred on a value to smooth,  
153 in order to replace that value with the mean, before moving the mask to the adjacent value. A larger  
154 mask results in a stronger applied smoothing function. If the dataset presents a strong background  
155 noise, it may be valid to repeat this step a second time, but it should be noted that if this option is  
156 performed, absolute values of concentration will not be accurate. The mean will be identical, but the  
157 absolute values of the extremes will no longer correspond to those given by initial data reduction and  
158 the map will therefore be semiquantitative. Relative fluctuations, however, will remain the same.

159

## 160 2.6 Detrending

161 The detrending option is useful in two different scenarios. Firstly, if a strong naturally-occurring trend  
162 is measured in the sample, the colour palette (commonly used to present fluctuation patterns) will  
163 only show this particular trend. Any higher frequency fluctuations along this trend or variations  
164 orthogonal to this direction (commonly observed in biominerals due to non-linear growth) and/or  
165 fluctuations of lower amplitude are thus invisible. Removing this main trend will allow qualitative  
166 study of such fluctuations. Additionally, if the background noise or sensitivity gradient is skewed as a  
167 result of experimental drift, a correction must be applied to stabilize the response across the elemental  
168 image. The technique presented here makes it possible to use data, even when a dramatic instrumental

169 drift occurs during an analytical session.

170 As is the case for smoothing, the process of detrending may change absolute values, so any  
171 interpretations can only be proposed for elemental distribution and relative fluctuations in  
172 concentration, in a semiquantitative fashion. Even in the case of naturally occurring trends, this option  
173 allows observation of lateral variations in concentrations that would otherwise be concealed.

174 The particular data set presented here shows a general trend of a supposedly decrease in Sr all along  
175 acquisition time, with data acquisition progressing in successive lines from left to right then top to  
176 bottom.

177 A first option to deal with this trend is to execute an automatic detrending. By clicking the  
178 corresponding button, AERYN calculates the best fitting linear plane to the data and applies a  
179 detrending corresponding to this plane.

180 Alternatively, to improve visibility in this case we can select a transect representative of the main  
181 fluctuation. By calculating the equation of the linear trend of this transect, it is possible to apply this  
182 equation as a correction to all lines (or columns) and reveal geochemical fluctuations across the entire  
183 map (Fig. 3). With this simple operation and even in the case of instrumental drift, it is possible to  
184 work on the map without necessarily having to return to data acquisition.

185 When selecting a line or a column and clicking on "Display", two new windows present the selected  
186 transect and its calculated linear trend on one panel (Fig. 3a), and the same transect along with its  
187 detrended transect on the other (Fig. 3b). No operations to the map have been done at this stage. If  
188 satisfied with these detrending parameters, the user can close both computer windows and Validate.

189 This will detrend the matrix and display the detrended map on all graphs (Fig. 3c). If the calculated  
190 transects are not satisfactory, they can be cancelled by resetting the detrending operation.

191 The corrected map now presents fluctuations in Sr which are visible as coherent bands both at the top  
192 and bottom of the map, showing continuity of these features. The map can be smoothed to clean the  
193 high-frequency fluctuations using a 5x5 mask (Fig. 4).

194

## 195 2.7 Export map

196 At any stage, it is possible to export the matrix. In order to maintain optimum picture quality, the

197 maps are exported as TIFF files without compression with a uniform size of both dimensions of the  
198 map. The user is asked to enter the path and file names. The matrix itself and the historic record of  
199 operations made are saved as tab delimited text files, and the data are subsequently importable in  
200 AERYN for further modification if required.

201 Figure 5 presents the Sr map used as an example here as well as a Li map from the same acquisition  
202 session after data reduction (Iolite v. 3.0) and after post-processing using AERYN. Whereas maps  
203 processed only with data reduction software are noisy and hamper visibility of concentration bands,  
204 these bands are clearly visible after processing with AERYN. If required, in order to counteract the  
205 standardization of the dimension of the map after saving with AERYN, it is possible to import the  
206 TIFF file in another image software (e.g., Adobe Photoshop) to resize the image to the proper aspect  
207 ratio.

208

### 209 3. Example materials

210 Specimens of the cold water coral *L. pertusa* were prepared at Trinity College Dublin using the  
211 protocols described in Mouchi et al. (2014). Cleaned aragonitic skeletons were embedded in epoxy  
212 resin and cut longitudinally with a Buehler Isomet Low Speed Saw. Sections obtained were polished  
213 and subsequently etched with 2 % formic acid for 50 s. The etching protocol allowed direct  
214 acquisition of measurements on LA-ICP-MS without pre-ablation.

215

#### 216 3.1 LA-ICP-MS

217 Geochemical data were collected using an Analyte Excite 193 nm excimer ArF\* laser ablation system  
218 (Photon-Machines Inc.) coupled to an iCAP-Q ICP-MS unit (Thermo Scientific) at the Trinity  
219 College Dublin geochemistry facility. Details on the instrument setup for elemental mapping can be  
220 found in Ubide et al. (2015). Parallel and slightly overlapping (1  $\mu\text{m}$ ) line scans were acquired as  
221 suggested by Ubide et al. (2015) to avoid gaps during data acquisition without notable contamination  
222 from adjacent lines. A square beam of 12  $\mu\text{m}$  was selected with 10 Hz repetition rate at 8  $\mu\text{m}\cdot\text{s}^{-1}$  scan  
223 speed and a laser fluence of 3.9  $\text{J}\cdot\text{cm}^{-2}$ . Ion intensities of  $^7\text{Li}$ ,  $^{43}\text{Ca}$ ,  $^{86}\text{Sr}$  and other isotopes not  
224 discussed here were measured for a total dwell time of 146 milliseconds. Individual dwell times were



225 70 ms for  $^7\text{Li}$ , 5 ms for  $^{86}\text{Sr}$  and 10 ms for  $^{43}\text{Ca}$ . Data acquisition procedures ran for a total of 2.5 h.  
226 Either NIST SRM 610 or NIST SRM 612 was ablated for approximately 120 s using the same  
227 ablation parameters as the unknown line scans. Two calibration lines were used at the beginning and  
228 end of each experiment and one additional line every 10 unknown sample lines which equates to 120 s  
229 of data acquisition on the reference material every approximately 25 minutes. Collected data were  
230 then processed for quantitative values with the Iolite software (Paton et al., 2011; v. 2.5 and 3.0) using  
231 the Trace\_Elements data reduction scheme (included in the Iolite program package) and the recently  
232 accepted values of NIST SRM 610 and NIST SRM 612 (Jochum et al., 2011).  $^{43}\text{Ca}$  was used as the  
233 internal standard, assuming a stoichiometric Ca content. Reduced data were then exported to be  
234 readable and further treated by AERYN; instructions to export text files readable by AERYN from  
235 Iolite are in the "Read Me" file provided as supplementary material.  
236 Depending on the size of the acquisition area for each specimen, typical maps have between 950 and  
237 1950 columns for 30 to 60 lines, corresponding to approximately 1-2 mm by 330-660  $\mu\text{m}$ ,  
238 respectively.  
239 The description of AERYN presented above (Fig. 1-5) used the map of distribution of Sr in *L. pertusa*  
240 as example. The map of distribution of Li (Fig. 6a) does not require the outlier removal step as the  
241 Side View indicates that the majority of measured fluctuations are below the resin value (see the  
242 arrows on Fig. 6a) and visible. Indeed, though some positive outliers are present on the right-hand  
243 side, they do not prevent reading of the minimum and maximum values on the histogram for palette  
244 definition. The map is however difficult to interpret in terms of the location of fluctuations in Li  
245 concentrations. The top part of the map is depleted in Li, as indicated by blue areas in opposition to  
246 red and yellow areas on the lower part of the map. An automatic detrending applied to reduce the  
247 amplitude of the fluctuations from top to bottom (Fig. 6b) aids in the visualization of several areas of  
248 higher and lower Li concentration oriented N-S in this view.  
249 From this step, a light smoothing using a 3 by 3 points mask further highlights the fluctuations. A  
250 wider mask was not chosen due to the reduced number of lines in this map (only 30). Except for the  
251 high value areas (in red) on the rightmost part of the map, both the map and the Side View show  
252 higher amplitudes of fluctuations on the left-hand part compared to the right-hand part of the map

253 (Fig. 7). As this side of the coral skeleton displaying elevated elemental concentrations corresponds to  
254 the initial stage of skeletal growth, this map can be interpreted in terms of environmental forcing or  
255 kinetic incorporation, as suggested by Mouchi et al. (2014) from a simple transect (i.e. the elemental  
256 variation of Li shown here is real and not an analytical or data processing artefact).

257

### 258 3.2 Electron microprobe

259 Another *L. pertusa* specimen was mapped with a Cameca SX-*Five* electron microprobe at the  
260 Camparis Service, Paris, France. Acquisition parameters were 15 keV, 200 nA, 500 ms dwell time per  
261 point with a 4  $\mu\text{m}$  beam diameter and step size on a surface of 580 by 1352  $\mu\text{m}$ . The map presented  
262 here corresponds to Mg wt% (Fig. 8) after calibration using internal reference materials for each  
263 measurement. The analytical uncertainty for this element using this protocol is approximately 100  
264  $\mu\text{g}\cdot\text{g}^{-1}$  (2 SD).

265 Although a dwell time of 500 ms was used for this analytical protocol, which is high compared to  
266 common trace element mapping protocols (usually set at around 300 ms), fluctuations in Mg  
267 concentrations are still difficult to observe (Fig. 8a) and seem to be lower than the 100  $\mu\text{g}\cdot\text{g}^{-1}$   
268 uncertainty. The visibility of these subtle fluctuations in Mg concentration can be improved using  
269 AERYN (Fig. 8b).

270 The corresponding export files were written with transposed matrices compared to the ones generated  
271 by Iolite. The "Transpose" button in AERYN was used to get the same orientation as for the LA-ICP-  
272 MS maps. After filtering the data to cut the outliers, the map remains very noisy due to low  
273 concentration values. We applied a 7x7 mask to strongly reduce the high-frequency fluctuations and  
274 applied a weak detrending as the first lines presented lower values. The resulting map is shown in  
275 Figure 8b.

276

277 The limits of the bands of high and low concentrations remain difficult to establish, but AERYN  
278 permits areas of lower concentrations within high concentration bands to be more clearly visualized,  
279 in particular around columns number 40, 80, 170 and 225. The map is therefore ready for  
280 interpretation. High concentration bands are wider on the left-hand side (corresponding to the initial

281 stages of skeletal growth) than on the right-hand side of the map. Whereas a detailed interpretation of  
282 the geochemical variations presented in these maps is beyond the scope of this paper, if Mg  
283 incorporation is, as Sr incorporation, governed by kinetics in the skeleton of *L. pertusa*, this  
284 observation would indicate in the present dataset that early stages of skeletal growth may feature  
285 enhanced growth fluctuations. The large bands of high Mg concentration also tend to indicate that  
286 most of these early stages present high growth rates and that the low growth rate periods are  
287 temporally extremely restricted. These observations are in accordance of those of Mouchi et al. (2014)  
288 and Rollion-Bard & Blamart (2015).

289

#### 290 4. Conclusion

291 AERYN uses data generated from micro-analytical techniques and processed by data reduction  
292 software (such as Iolite) to improve the interpretation of elemental distribution maps. This paper has  
293 presented an alternative way to the trial-and-error routine of modification of palette thresholds by  
294 allowing the user to display the geochemical dataset in 3D and observe data extremes systematically.  
295 Moreover, AERYN allows the user to counteract any apparent changes due to instrumental drift,  
296 which might not be possible to correct with traditional data reduction schemes. AERYN makes it  
297 possible to observe discrete areas of high or low concentration which may be hidden by natural strong  
298 fluctuations or analytical artefacts.

299 This program can highlight subtle variations in elemental maps in just a couple of minutes, thereby  
300 enhancing the interpretation of elemental maps obtained with a variety of analytical techniques such  
301 as LA-ICP-MS, EPMA and SEM-EDS.

302

#### 303 Acknowledgements

304 The work presented in this paper was made possible by the ENS Ph.D. programme. The Earth and  
305 Natural Sciences Doctoral Studies Programme is funded under the Programme for Research in Third-  
306 Level Institutions Cycle-5 and co-funded under the European Regional Development Fund. The  
307 authors would like to thank Cora McKenna for her help operating the LA-ICP-MS, and Eric P.  
308 Verrecchia for his advice on some algorithms for the code of AERYN. John D'Errico kindly offered

309 the use of his Matlab function `inpaint_nans`. We acknowledge detailed feedback from one reviewer  
310 and the editor which helped us improve the original version of the manuscript.

311

## 312 References

313 Carling, K., 2000. Resistant outlier rules and the non-Gaussian case. *Comput. Stat. Data. An.* 33, 249-  
314 258.

315 Cusack, M., Dauphin, Y., Cuif, J.-P., Salomé, M., Freer, A., Yin, H., 2008. Micro-XANES mapping  
316 of sulfur and its association with magnesium and phosphorus in the shell of the brachiopod,  
317 *Terebratulina retusa*. *Chem. Geol.* 253, 172-179.

318 D'Errico, J., 2004. `inpaint_nans`. MATLAB Central File Exchange. Retrieved October, 20, 2014.

319 Jochum, K.P., Weis, U., Stoll, B., Kuzmin, D., Yang, Q., Raczek, I., Jacob, D.E., Stracke, A.,  
320 Birbaum, K., Frick, D.A., Günther, D., Enzweiler, J., 2011. Determination of reference values for  
321 NIST SRM 610-617 glasses following ISO guidelines. *Geostand. Geoanal. Res.* 35, 397-429.

322 McGowan, N., Fowler, A.M., Parkinson, K., Bishop, D.P., Ganio, K., Doble, P.A., Booth, D.J., Hare,  
323 D.J., 2014. Beyond the transect: An alternative microchemical imaging method for fine scale analysis  
324 of trace elements in fish otoliths during early life. *Sci. Total Environ.* 494-495, 177-186.

325 Mouchi, V., Crowley, Q.G., Jackson, A.L., McDermott, F., Monteys, X., de Rafélis, M., Rueda, J.L.,  
326 Lartaud, F., 2014. Potential seasonal calibration for palaeoenvironmental reconstruction using skeletal  
327 microstructures and strontium measurements from the cold-water coral *Lophelia pertusa*. *J.*

328 *Quaternary Sci.* 29, 803-814.

329 Ortolano, G., Zappalà, L., Mazzoleni, P., 2014. X-Ray Map Analyzer: A new ArcGIS based tool for  
330 the quantitative statistical data handling of X-ray maps (Geo- and material-science applications).  
331 *Comput. Geosci.* 72, 49-64.

332 Paton, C., Hellstrom, J., Paul, B., Woodhead, J., Hergt, J., 2011. Iolite: Freeware for the visualisation  
333 and processing of mass spectrometric data. *J. Anal. Atom. Spectrom.* 26, 2508-2518.

334 Paul, B., Paton, C., Norris, A., Woodhead, J., Hellstrom, J., Hergt, J., Greig, A., 2012. CellSpace: A  
335 module for creating spatially registered laser ablation images within the Iolite freeware environment.  
336 *J. Anal. Atom. Spectrom.* 27, 700-706.

337 Paul, B., Woodhead, J.D., Paton, C., Hergt, J.M., Hellstrom, J., Norris, C.A., 2014. Towards a method  
338 for quantitative LA-ICP-MS imaging of multi-phase assemblages: mineral identification and analysis  
339 correction procedures. *Geostand. Geoanal. Res.* 38, 253-263.

340 Petrus, J.A., Kamber, B.S., 2013. A novel 2D LA-ICP-MS data analysis and visualization solution.  
341 *Goldschmidt2013 Conference Abstracts*, 1959.

342 Rittner, M., Müller, W., 2012. 2D mapping of LA-ICPMS trace element distributions using R.  
343 *Comput. Geosci.* 42, 152-161.

344 Rollion-Bard, C., Blamart, D., 2015. Possible controls on Li, Na, and Mg incorporation into aragonite  
345 coral skeletons. *Chem. Geol.* 396, 98-111.

346 Tukey, J.W., 1977. *Exploratory Data Analysis*. Addison Wesley, Pennsylvania.

347 Ubide, T., McKenna, C.A., Chew, D.M., Kamber, B.S., 2015. High-resolution LA-ICP-MS trace  
348 element mapping of igneous minerals: in search of magma histories. *Chem. Geol.* 409, 157-168, doi:  
349 10.1016/j.chemgeo.2015.05.020.

350

### Figure captions

Figure 1: Main window of AERYN showing a Sr distribution map measured by LA-ICP-MS on a *Lophelia pertusa* specimen. Data were reduced in terms of baseline correction and standard calibration prior importation in AERYN. At this stage, no corrections have been applied.

Figure 2: Coral skeleton Sr content measured by LA-ICP-MS as line scans at the outlier removal step (colour bar represents concentration in  $\mu\text{g.g}^{-1}$ ) using Matlab's "surf" function. a: Map after filtering data out below 0 and above  $100,000 \mu\text{g.g}^{-1}$ . b: Side view rotated to expose the surface, showing the areas with the cut values in white (located by the arrows). c: Side view once the filtering has been validated. In order to retain the representative variability in the dataset, we advise not to cut the outliers below the values indicated here by the embedded red dashed line below which fluctuations do not appear anymore as discrete outliers. d: Final map and side view after removing outliers above  $20,000 \mu\text{g.g}^{-1}$  (corresponding to the red dashed line in c). At this stage, the histogram distribution can help to define the range for the colour palette (red dashed lines). The high count bin around  $0.6 \cdot 10^4 \mu\text{g.g}^{-1}$  corresponds to the resin value (i.e. not the biogenic carbonate) and is represented in dark blue on both sides of the map.

Figure 3: Detrending applied to the Sr distribution map. a: Selected transect from the map (in black) and calculated trend (in red). b: The original transect (black) and the detrended transect (red). c: Map after outlier removal and prior detrending is applied (compare to Fig. 2). d: Graphs obtained after detrending and rescaling palette range.

Figure 4: Sr distribution map after automatic detrending and smoothing with a 5 by 5 mask.

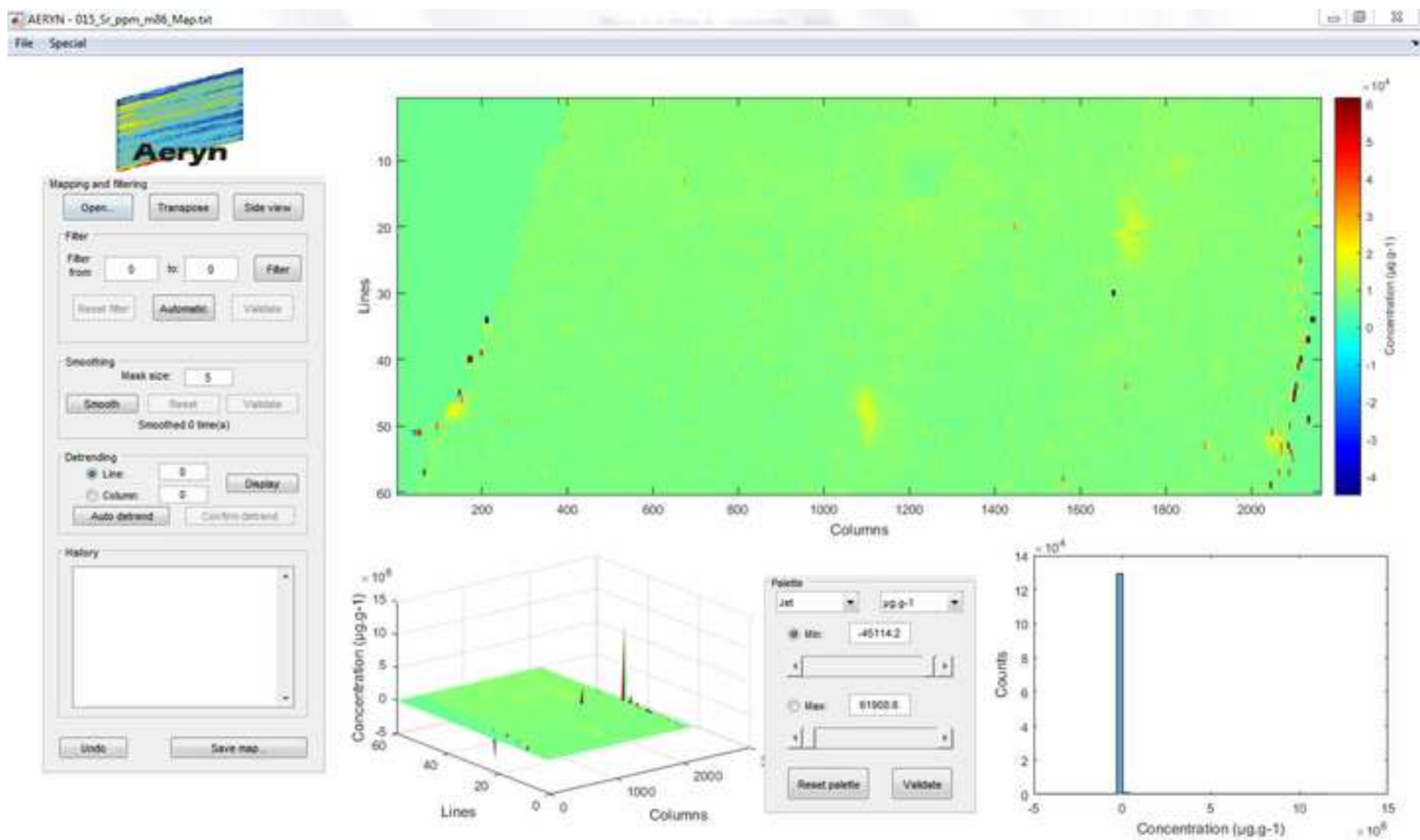
Figure 5: Element distribution maps resulting from data reduction using Iolite v. 3.0 (left) and after processing by AERYN (right) for Sr (a) and Li (b). Concentration bands are more clearly visible after processing with AERYN.

Figure 6: First steps for the Li map. a: Initial data after import of the Iolite export file. The resin is indicated by the arrows on the map and the Side View. b: Map after automatic detrending.

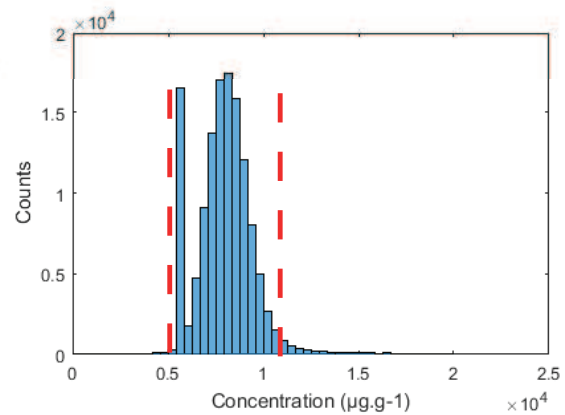
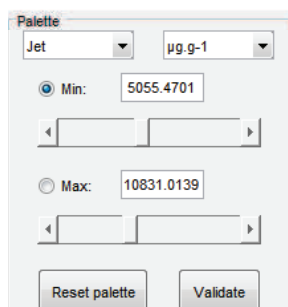
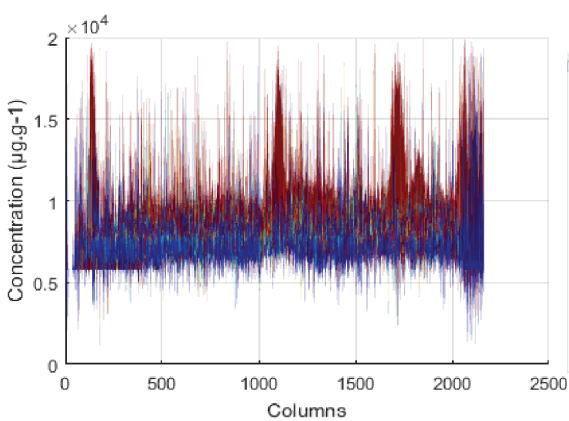
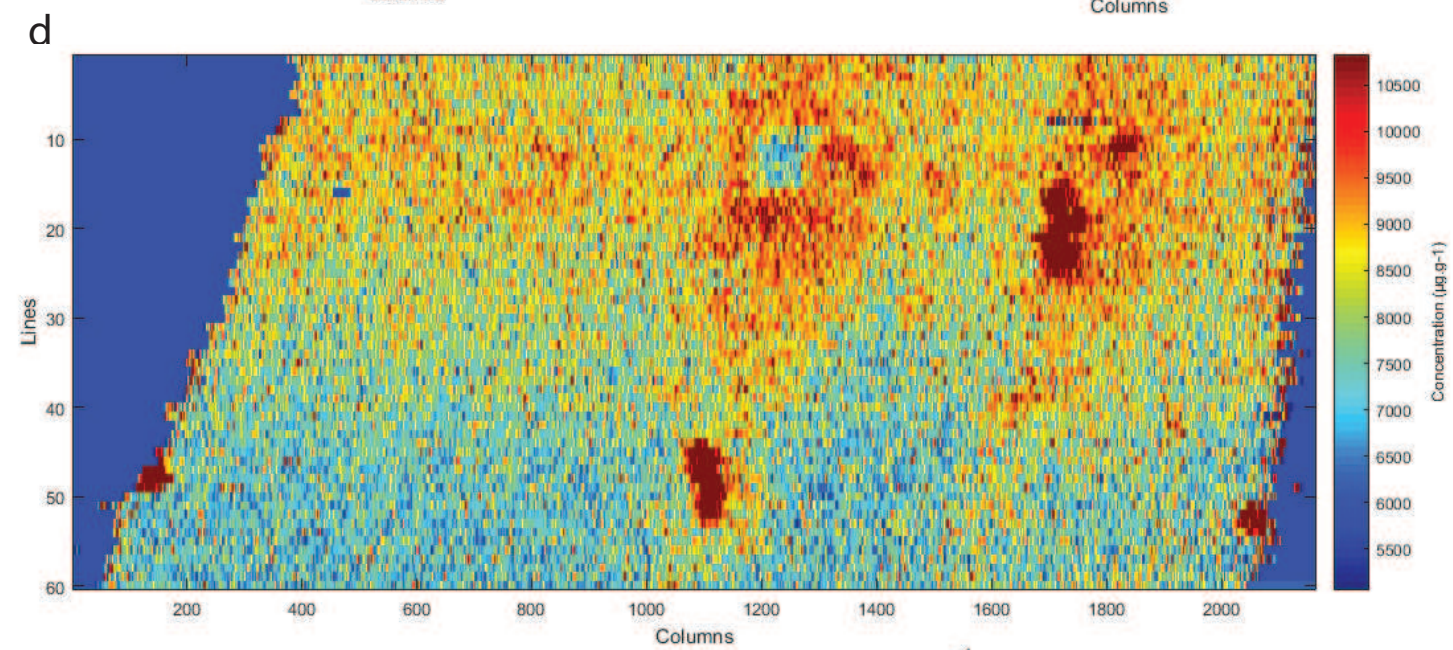
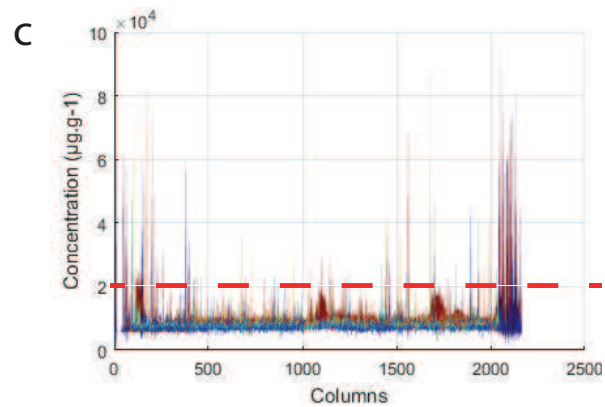
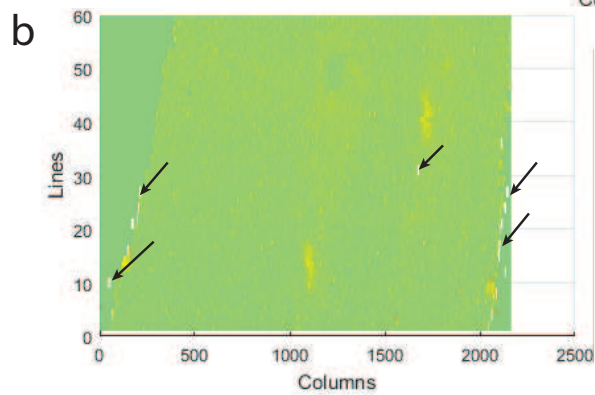
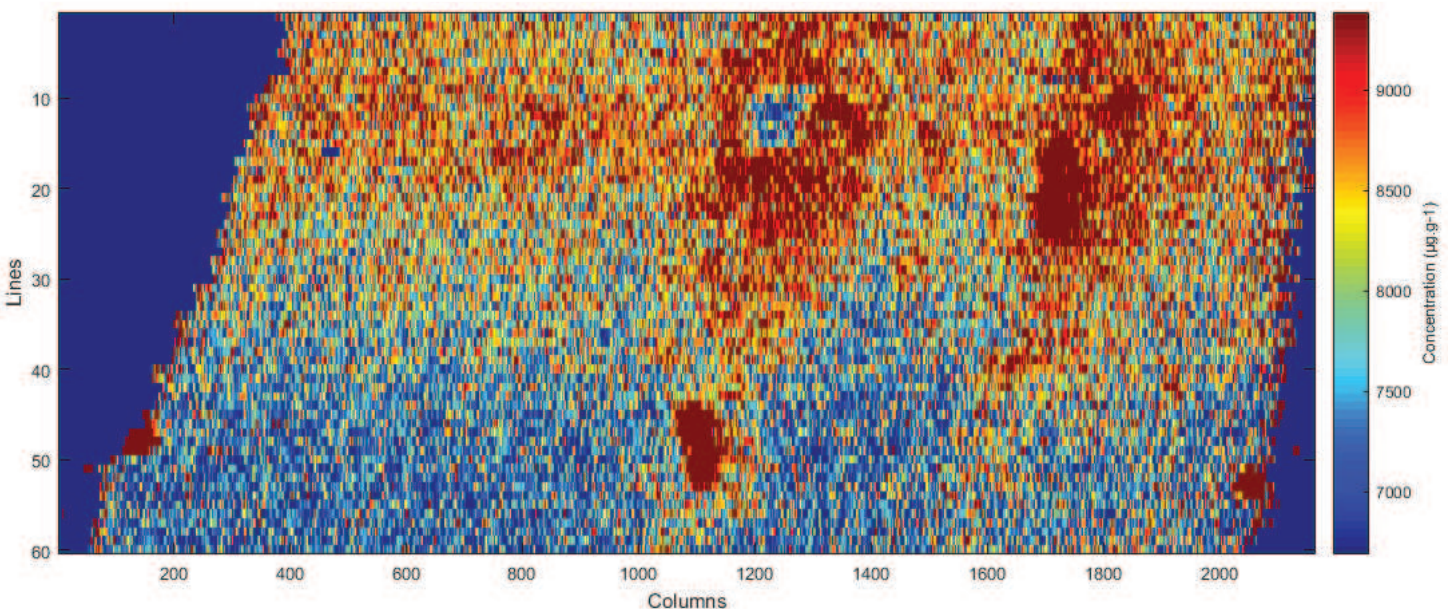
Figure 7: Smoothed map of Li concentration, using a 3x3 mask (each value replaced by the mean of all surrounding values in a 3 by 3 points area). Skeletal growth direction is right to left on this map.

Figure 8: Mg (wt.%) map of a *L. pertusa* specimen acquired by electron microprobe, as obtained by the SX acquisition software (a) and after processing with AERYN by smoothing using a 7x7 mask and detrending (b). Skeletal growth direction is left to right on this map.

Figure 1  
[Click here to download high resolution image](#)





**Figure 2**



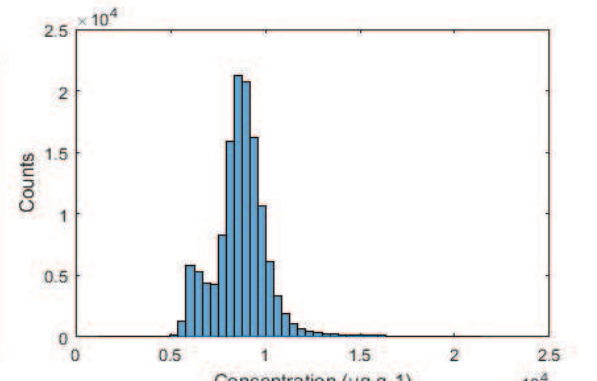
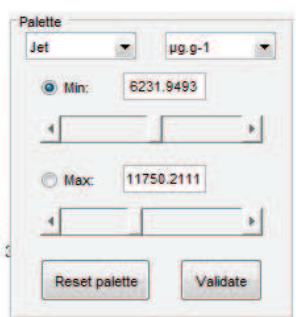
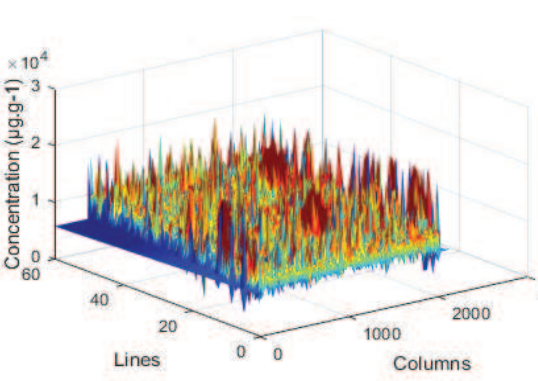
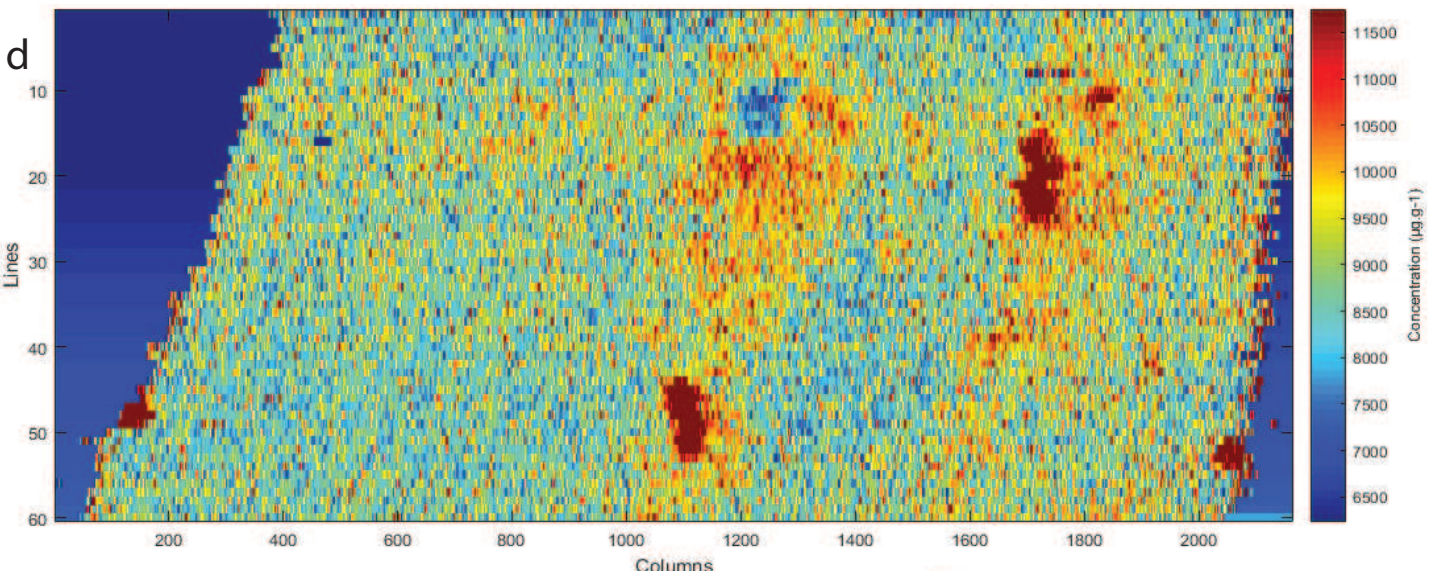
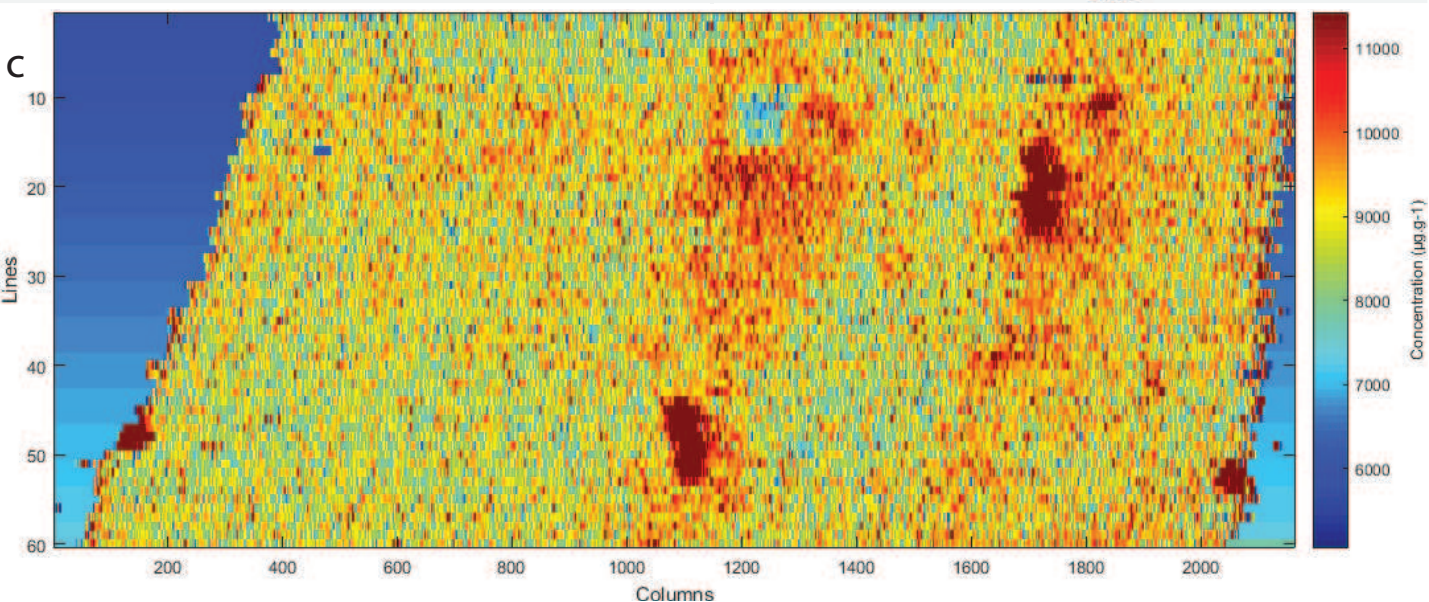
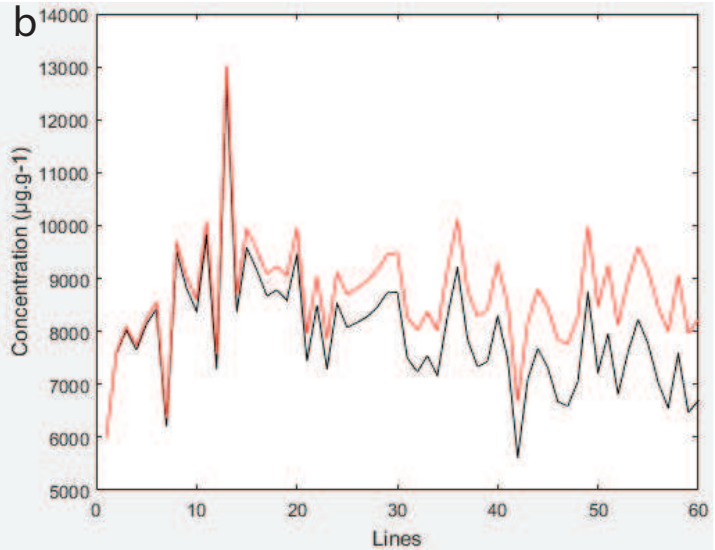
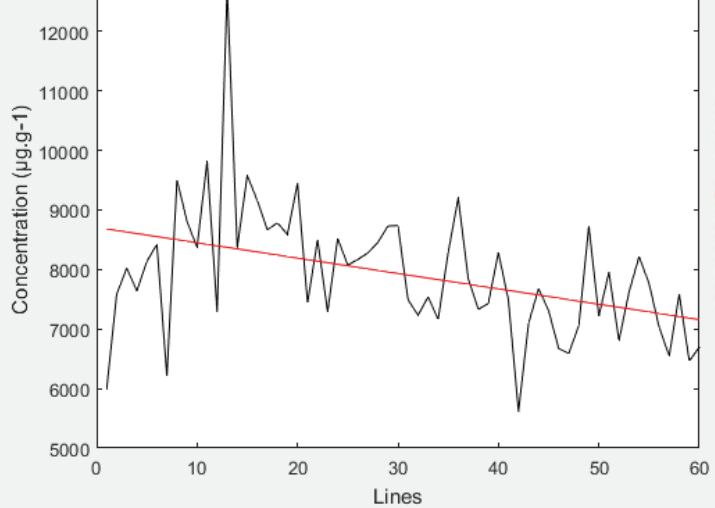
**Figure 3**



Figure 4  
[Click here to download high resolution image](#)

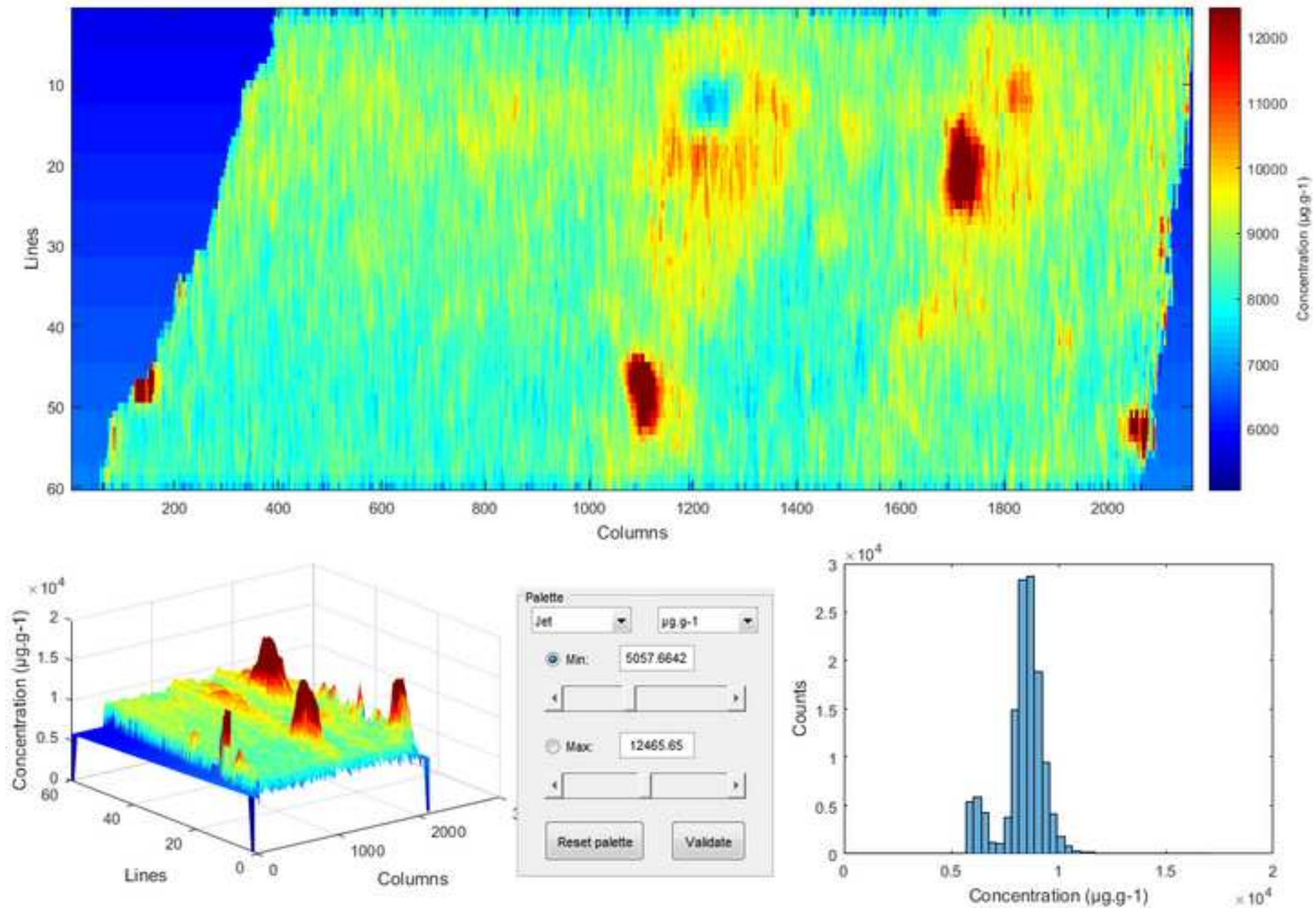


Figure 5

Pre-AERYN

Post-AERYN

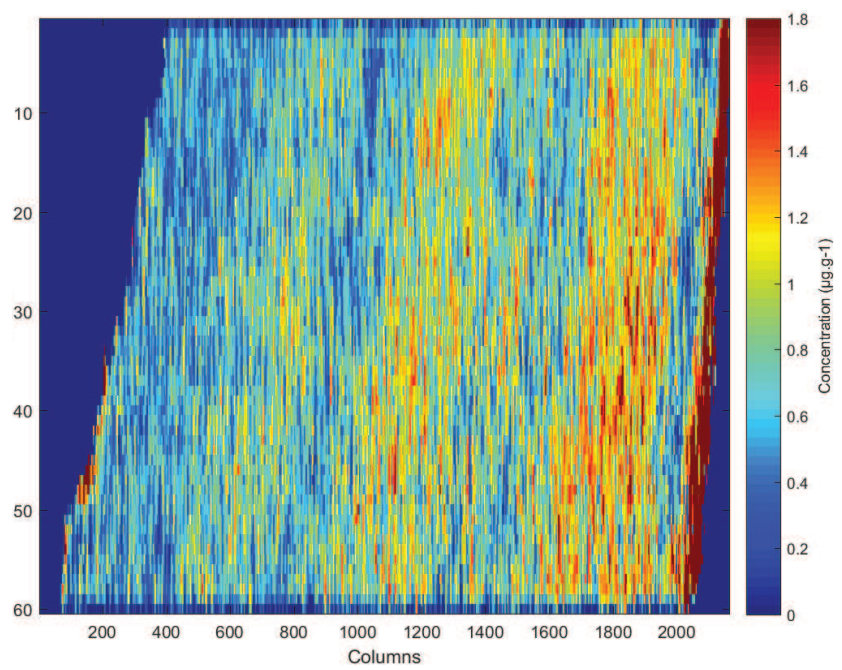
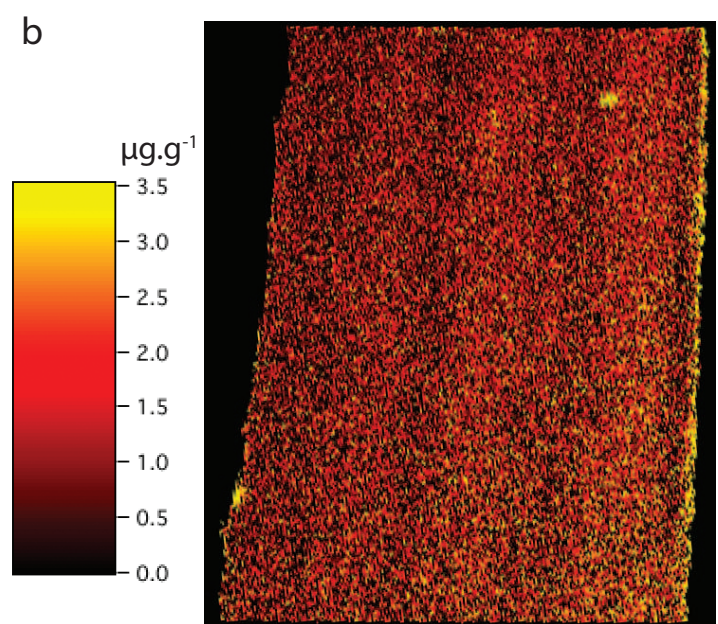
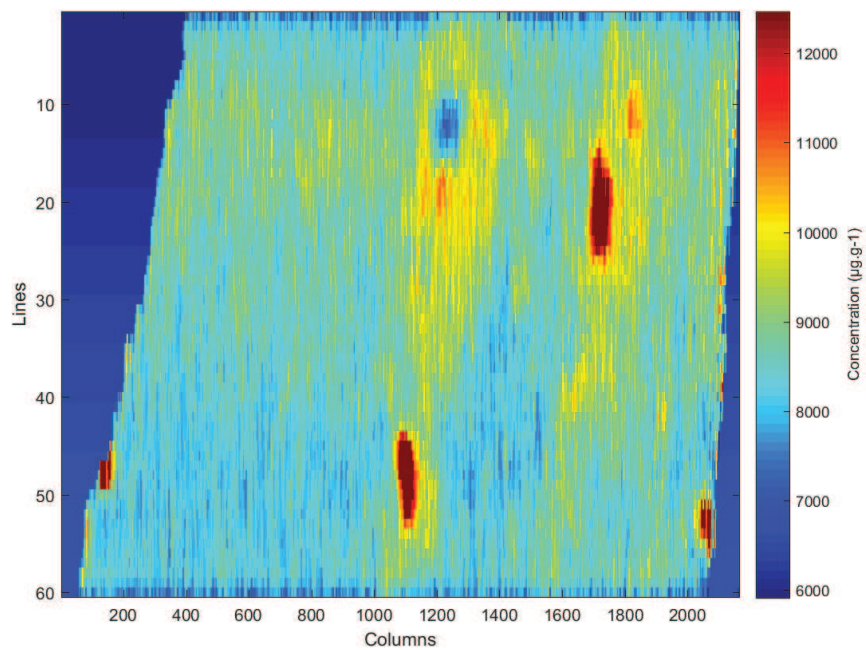
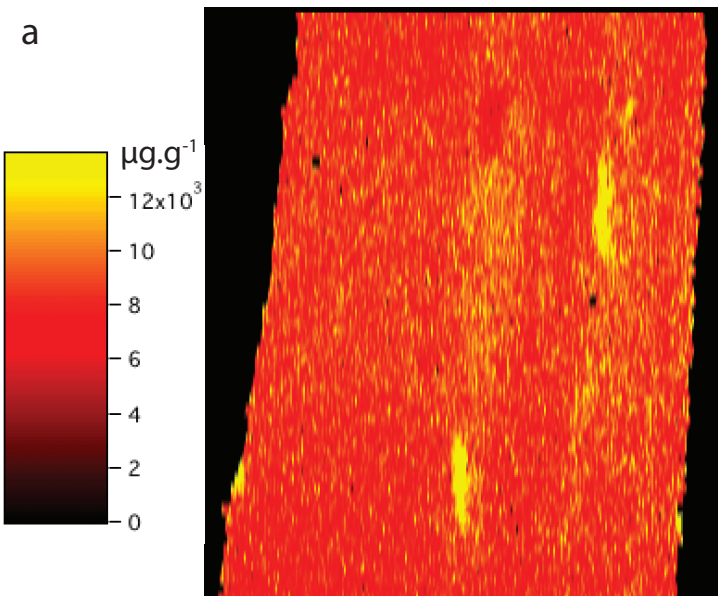
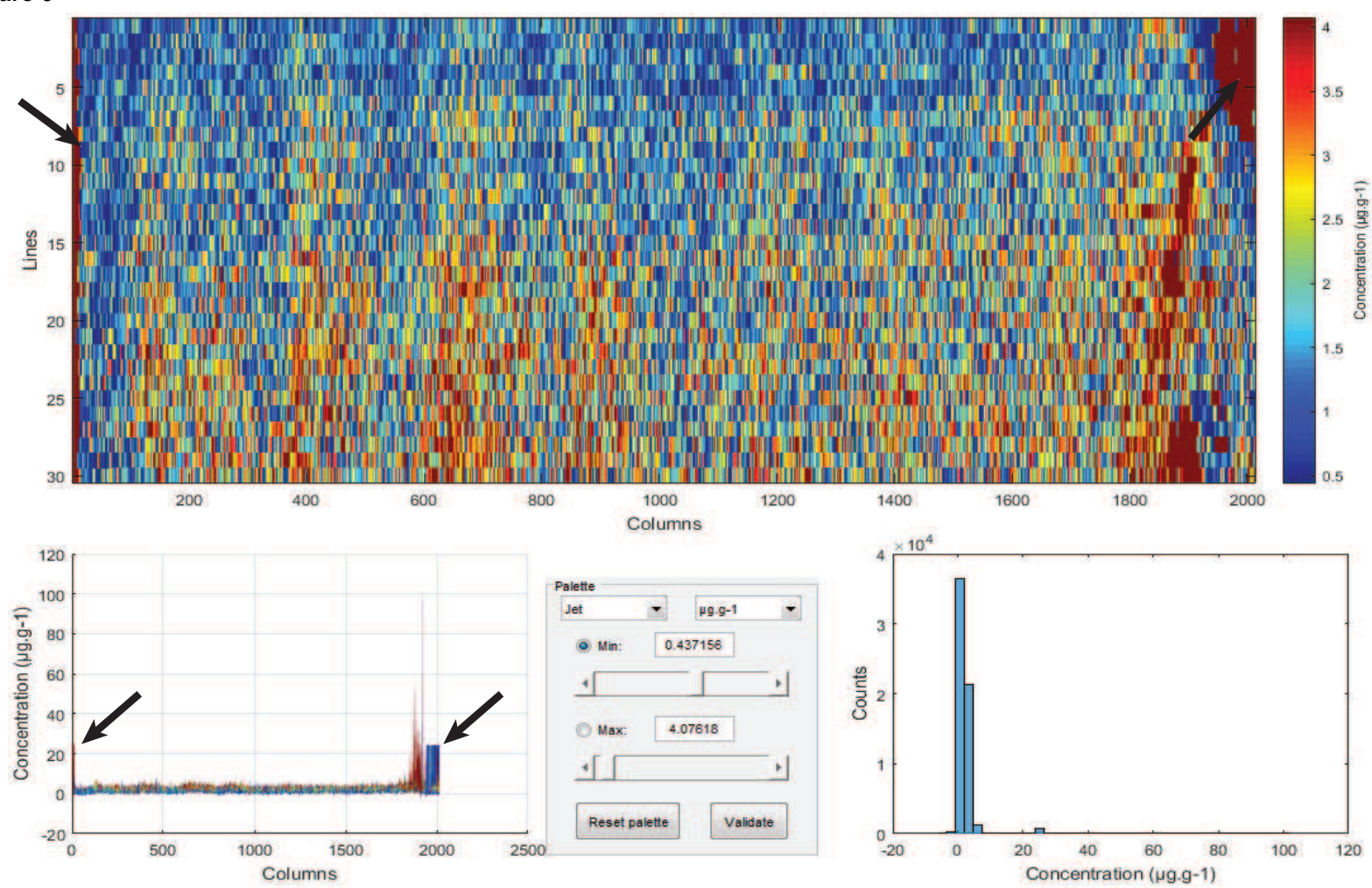




Figure 6

a



b

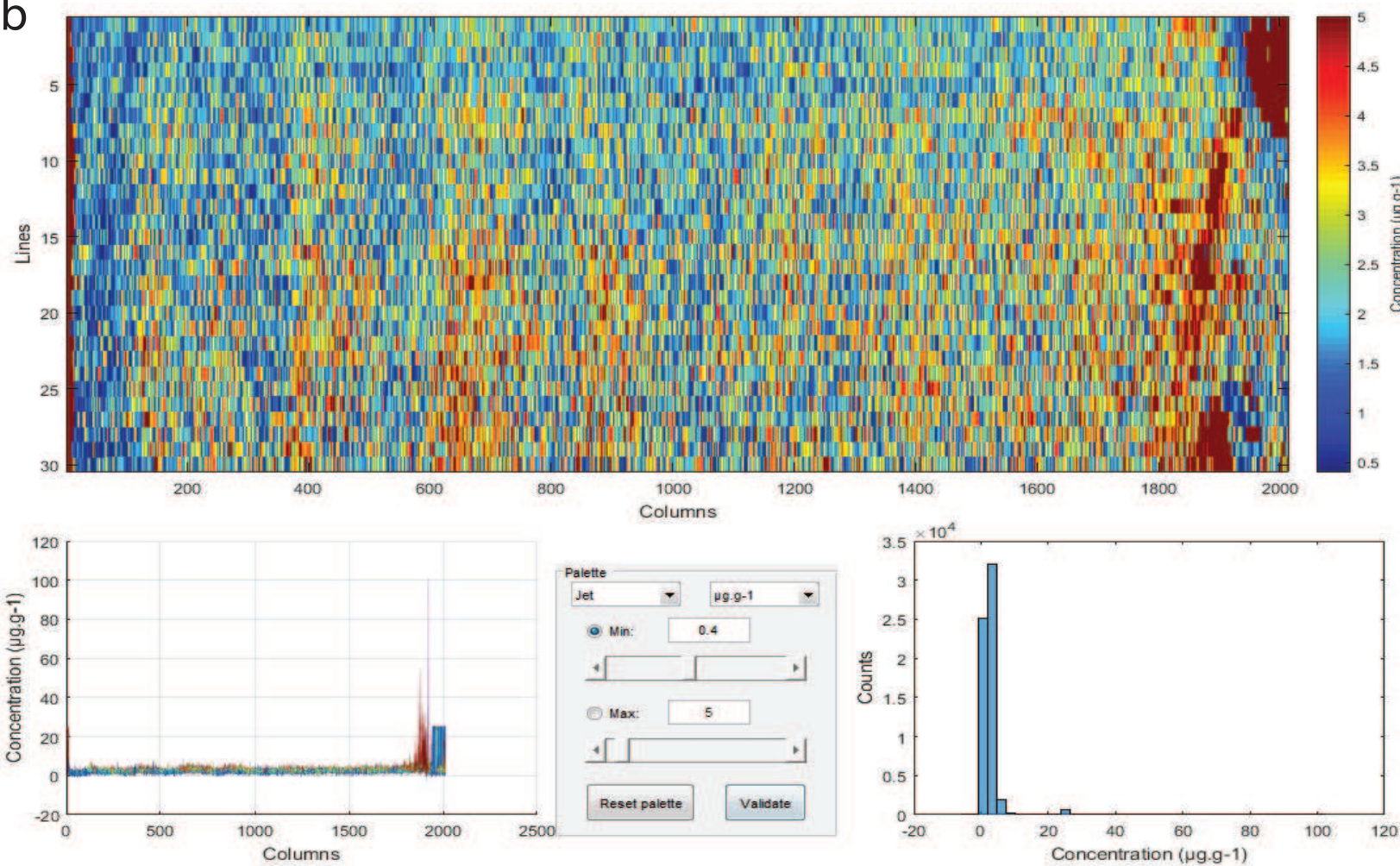




Figure 7

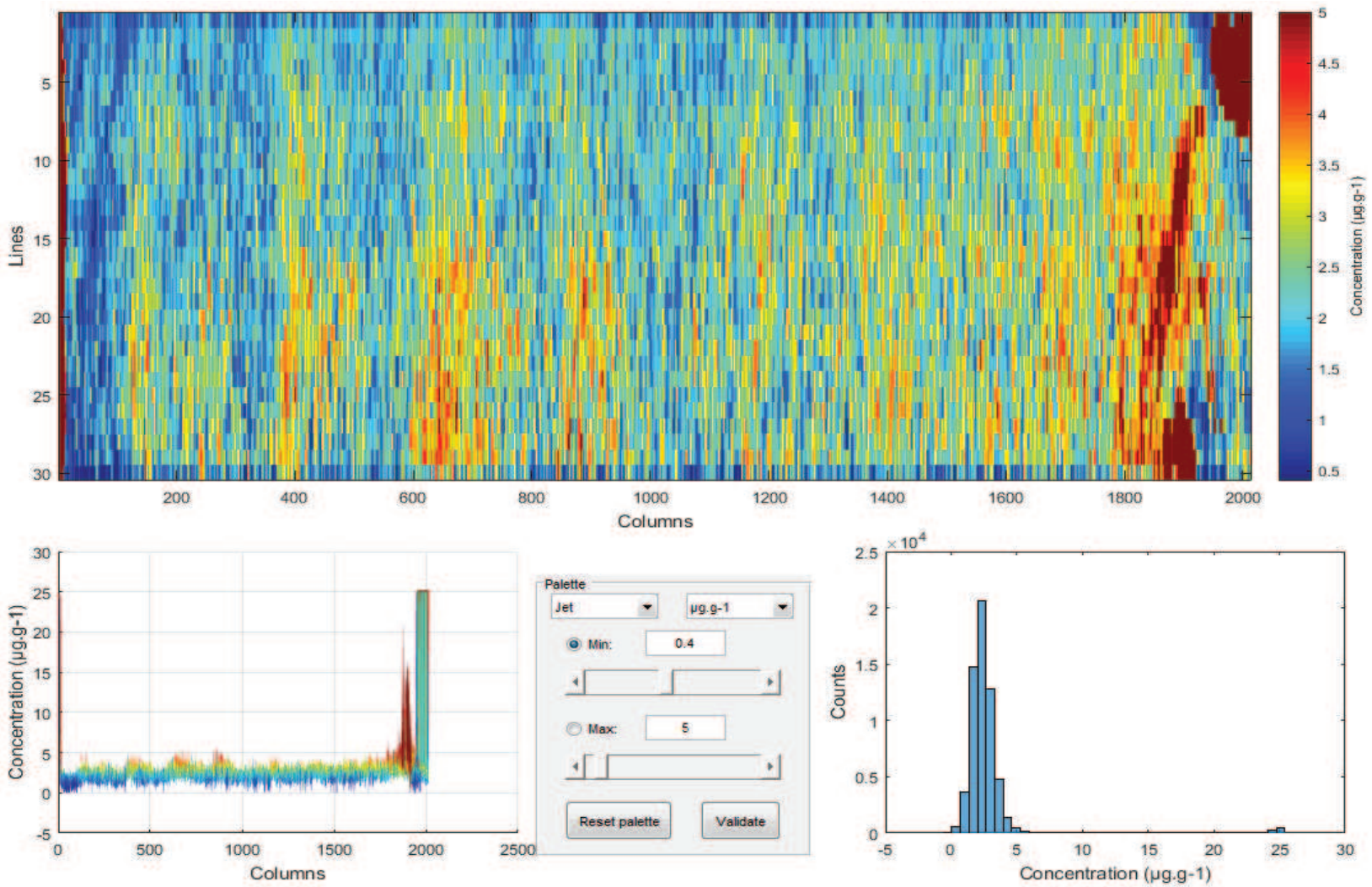


Figure 8

